

Dissociative electron attachment to acetylene

S. T. Chourou* and A. E. Orel

Department of Applied Science, University of California, Davis, Davis, California 95616, USA

(Received 29 January 2008; published 10 April 2008)

The mechanism and cross section for dissociative electron attachment of acetylene after collision with electrons in the 0–7 eV range is reported. The positions of the resonances and the autoionization widths are determined by electron scattering calculations using the complex Kohn variational method. The complex potential energy surface relevant to the metastable negative ion $C_2H_2^*$ is constructed as a function of the $C \equiv C$ and $C-H$ stretches and the CCH angle. The lowest resonant potential is then used as input for the study of the dissociation dynamics within the local complex potential model using the multiconfiguration time-dependent Hartree method. The calculated dissociative electron attachment cross section as a function of electron energy is compared to available experimental findings.

DOI: [10.1103/PhysRevA.77.042709](https://doi.org/10.1103/PhysRevA.77.042709)

PACS number(s): 34.80.Ht, 31.15.xv

I. INTRODUCTION

Acetylene is the smallest unsaturated hydrocarbon molecule. Studies on dissociative electron attachment (DEA) to this system are interesting since C_2H_2 has an unoccupied π orbital comparable to the isoelectronic N_2 molecule. Therefore, the study of the dissociation of the metastable negative ion of C_2H_2 may serve as a prototype to study polyatomic molecules characterized by a π^* -shape resonance.

Interest in electron-driven chemistry of acetylene spans a wide range of areas of research and applications. It is well established that presence of hydrocarbons in planetary atmospheres and interstellar media have a significant impact on the chemical processes taking place in these environments [1,2]. For example, acetylene has been detected in interstellar clouds with a wide range of abundances (see Lacy *et al.* [3], and references therein) and it has been suggested more recently that C_2H_2 is a key species in the prebiotic evolution on Titan [4]. An even more growing interest within the astrophysics community resulted from the discovery of acetylene along with hydrogen cyanide and carbon dioxide on IRS 46, a young star in the Ophiuchus constellation, and it is believed that these organic compounds play a major role as gaseous precursors for protein and partial DNA formation [5].

Moreover, acetylene, among other hydrocarbons, has been utilized in plasma processing in microtechnology and nanotechnology. Acetylene plasmas are commonly used for deposition of carbon thin films, more particularly diamondlike thin films of relevance in semiconductor, mechanical, and biomedical applications [6]. The chemistry of these plasmas, involving DEA among other processes, have been studied by Stoykov *et al.* [7]. Furthermore, it has been recently reported that C_2H_2 represents a highly efficient carbon feedstock for the growth of carbon filaments and nanotubes by plasma enhanced chemical vapor deposition [8]. Electron collision with C_2H_2 is therefore a key process that initiates and drives the formation of reactive species in cold plasmas. It is worth mentioning that acetylene also plays an important role in

combustion science and that the chemical processes involved thereby can be rather complex as discussed in [9]. Accurate calculations of the DEA mechanism and the resulting cross sections are thus required for a thorough understanding of these phenomena.

The acetylene molecule has been studied extensively in the literature both experimentally and theoretically; however, less work has been done on its negative ion and its decay. Early DEA experiments by Trepka and Neuert [10] produced a low resolution C_2H^- yield spectra displaying an intense band with an onset at 2.8 ± 0.2 eV and a weaker band with an onset at 6.0 ± 0.3 eV. Later measurements of DEA to acetylene by Azria and Fiquet-Fayard [11] revealed a π^* -shape resonance at 2.6 eV and a yield of C_2H^- characterized by a vertical onset at thermodynamic threshold 2.3 eV. They further observed a significant isotope effect by measuring a C_2D^- yield over one order of magnitude smaller than that of C_2H^- around the peak position at 2.55 eV. Abouaf *et al.* [12] achieved high resolution low-energy spectra and observed a yield of C_2H^- peaking around 3 eV with a vertical onset at 2.69 eV.

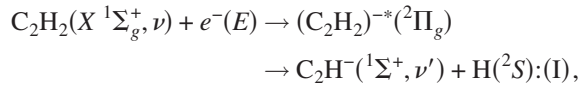
On the other hand, vibrational excitation (VE) experiments done by Andric and Hall [13] and Tronc and Malegat [14] investigating the resonance features in the $e^-C_2H_2$ collision system reported a π^* resonance at 2.6 eV as well as a σ^* resonance at 6.2 eV. Kochem *et al.* [15] treated in further detail VE to C_2H_2 in the 0–3.6 eV range and found the ${}^2\Pi_g$ transient negative ion state to lie at 2.6 eV.

Tossell [16] calculated the elastic electron scattering cross section of C_2H_2 using the continuum MS- $X\alpha$ approach. The maximum in the elastic cross section was found at 2.6 eV. Krumbach *et al.* [17] calculated the resonance positions and widths relevant to the ${}^2\Pi_g$ state of $C_2H_2^*$ as a function of $C \equiv C$ distance in linear geometry. They obtained a resonance at 2.9 eV for the equilibrium geometry. Gianturco and Stoeklin [18] found the resonance to lie at 2.5 eV from a scattering calculation employing a correlation-polarization potential model. Electron scattering from acetylene in the 0.01–20 eV energy range has been investigated by Jain [19] using close-coupling theory and including correlation and polarization effects reported a π^* -shape resonance at around 2 eV. Therefore, theoretical investigations of electron scatter-

*stchourou@ucdavis.edu

ing from acetylene are in good agreement with the experimental findings at energies below 5 eV.

Allan and Dressler [20] carried out a more complete study of the temporary $C_2H_2^*$ and its dissociation using electron transmission spectroscopy and energy-loss measurements. The 0–3 eV collision energy range led predominantly to production of H and C_2H^- fragments in their ground electronic states. The corresponding DEA cross section shows a pronounced peak around 3 eV with a nonvertical onset at around 2.6 eV. Recent experiment [21] produced higher resolution measurements of the absolute DEA cross section which was found to have a maximum of about 3.65 pm^2 at 2.95 eV electron energy. The authors in [11,20,21] further concluded, based on symmetry arguments, that $C_2H_2^*$ predissociated in bent geometry. In fact, the DEA process studied in the present work is given by the following mechanism:



which suggests that a symmetry breaking event takes place along this reaction pathway. Note that the initially formed negative ion is a π^* -shape resonance in its ${}^2\Pi_g$ symmetry and thus does not correlate with the fragments $C_2H^-({}^1\Sigma^+)$ and $H({}^2S)$ in their totally symmetric representations. This implies that a one-dimensional study of this system is inadequate to describe the dissociation dynamics and that molecular bending must be taken into consideration. This is similar to what was seen in earlier studies of DEA in formic acid [22]. In this system the dissociation dynamics were found to be intrinsically polyatomic, the anion was forbidden from dissociating to the observed fragments in planar geometry, and found to deform to nonplanar geometries before fragmenting. A second anion surface, connected to the π^* surface through a conical intersection, was involved in the dynamics. In this study we investigate the decay dynamics of the metastable $C_2H_2^*$, following the dissociation and studying how the collision energy channels between the internal degrees of freedom leading to the observed products in the 3 eV range.

The first section of this paper presents the theoretical approach and the computational techniques we used to calculate the adiabatic potential energy surfaces (APES) associated with the ground electronic state of the neutral C_2H_2 target. In this section, we further describe the electron scattering calculation performed to determine the resonant states and construct the complex APES. In the second section, we outline the multiconfiguration time-dependent Hartree (MCTDH) method and study the nuclear dynamics for acetylene using the calculated APES. Finally, we report the resulting DEA cross sections and branching ratios relevant to the $C \equiv C$ vibrational modes of the C_2H^- fragment.

II. POTENTIAL ENERGY SURFACES

A. *Ab initio* methods

1. Neutral target

In order to determine the initial vibrational states of the neutral target, we seek to construct the APES relevant to the

initial electronic state of the molecule as a function of its internal degrees of freedom. In this study, we perform electronic structure calculation using multiconfiguration self-consistent field (MCSCF) approach followed by a multireference configuration interaction (MRCI) calculation all for various geometries of the molecule. The carbon and hydrogen atoms were described using a triple-zeta-plus-polarization basis. The C_2H_2 function basis set is then augmented with three *s* diffuse functions (with exponents 0.05 centered on the carbons and 0.08 and 0.033 centered on the hydrogens) and three *p* diffuse functions (with exponents 0.02 centered on the carbons and 0.2 and 0.05 centered on the hydrogens). The MRCI calculation is carried out by freezing four core electrons and including single excitations in an active space of 20 molecular orbitals.

2. Resonant states of the ion

Electron collision with the neutral target leads to formation of a short-lived negative ion or resonant state. Since this state is embedded in the continuum, we carry out electron scattering calculations to determine both the resonance energies ϵ_{res} and the autoionization widths Γ as a function of the molecules internal coordinates.

We use the complex Kohn variational method [23] where in a first approximation (static exchange level), we neglect the polarization and correlation effects so that the $(n+1)$ -electron scattering wave function for fixed nuclei positions represented collectively by the vector \mathbf{Q} reduces to

$$\phi_{el}^\lambda(\mathbf{r}^{n+1}; \mathbf{Q}) = \hat{A} \left(\sum_{\lambda'} \phi_{el}^{\lambda'}(\mathbf{r}^n; \mathbf{Q}) F^{\lambda\lambda'}(\vec{r}_{n+1}; k) \right), \quad (1)$$

where $\mathbf{r}^{n+1} = (\vec{r}_1, \vec{r}_2, \dots, \vec{r}_{n+1})$ is the $(n+1)$ -electronic coordinates vector, \hat{A} is the antisymmetrizing operator. The function $\phi_{el}^\lambda(\mathbf{r}^n; \mathbf{Q})$ is the target n -electron ground state in the irreducible representation λ with the nuclei clamped at \mathbf{Q} . $F^{\lambda\lambda'}(\vec{r}_{n+1}; k)$ is the scattering electron's wave function at position \vec{r} and momentum k , which is further expanded to match asymptotic boundary conditions,

$$F^{\lambda\lambda'}(\vec{r}; k) = \sum_i c_i^{\lambda\lambda'} u_i(\vec{r}) + \sum_{lm} [f_l^\lambda(kr) \delta_{ll'} \delta_{mm'} \delta_{\lambda\lambda'} \\ + T_{ll'mm'}^{\lambda\lambda'}(k) h_l^{+\lambda}(kr)] Y_{lm}(\hat{r})/r, \quad (2)$$

where the $\{u_i\}_i$ are square-integrable functions, $\{f_l^\lambda\}_l$ and $\{h_l^{+\lambda}\}_l$ are, respectively, the regular Ricatti-Bessel and the outgoing Hankel functions and Y_{lm} are the normalized spherical harmonics. The terms $T_{ll'mm'}^{\lambda\lambda'}$ are the T -matrix elements that we are seeking to determine in order to compute the eigenphase sums as a function of the electron's collision energy. By fitting the eigenphase sums to the Breit-Wigner form, we determine the resonance parameters $\epsilon_{\text{res}}^\lambda$ and Γ^λ . The present system exhibits more than one resonance as will be demonstrated in the next section; therefore, the fitting procedure will involve the sum of multiple Breit-Wigner functions,

$$\delta_{\text{sum}}\left(\frac{k^2}{2}\right) = \sum_{p=1}^{N_{\text{res}}} \arctan\left(\frac{\Gamma_p^\lambda/2}{\epsilon_{\text{res},p}^\lambda - \frac{k^2}{2}}\right) + \delta_{\text{bkgd}}\left(\frac{k^2}{2}\right); \quad (3)$$

where N_{res} is the number of overlapping resonances, $(\epsilon_{\text{res},p}^\lambda, \Gamma_p^\lambda)$ are the corresponding parameters to be determined, and δ_{bkgd} is the background phase shift taken to be a slowly varying function of the electron energy.

B. Computational results

In its electronic ground state, acetylene has linear geometry and belongs to the $D_{\infty h}$ point group. The electronic structure calculation provides the molecular orbitals; hence, the electronic configuration of the ground state

$$(X^1\Sigma_g^+)1\sigma_g^2 1\sigma_u^2 2\sigma_g^2 2\sigma_u^2 3\sigma_g^2 1\pi_u^4.$$

Since in this work we address the DEA channel described by (I), we are interested in taking into account the dissociative coordinate of only one of the hydrogen atoms in C_2H_2 . Therefore, we have chosen to describe the geometries of acetylene using Jacobi coordinate shown in Fig. 1(b) where R represents the distance between H and the center of mass of linear C_2H .

The first series of calculations (series of calculations refer to a set of electronic structure calculation and scattering calculation) were carried out in quasilinear geometry where the CCH is bent by an angle of 1° . This is achieved in order to keep consistency of the functional basis sets when perform-

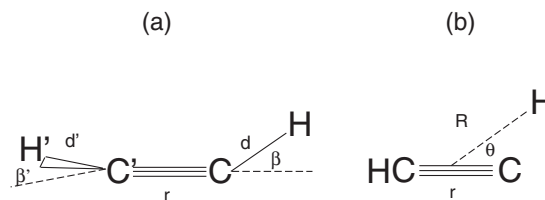


FIG. 1. Coordinates used for nonplanar geometry calculations (a) and Jacobi coordinates used in DEA dynamics calculation (b).

ing calculations in lower symmetries of the molecule. The electronic structure calculation in this bent geometry using the MCSCF and MCRI methods outlined in the preceding section resulted in a total of 15 064 configurations. The one-dimensional potential for the neutral target is constructed for $R \in [2.5 \text{ a.u.}, 7.0 \text{ a.u.}]$ in the A' irreducible representation where the electronic configuration is given by

$$(X^1A')1a'^2 2a'^2 3a'^2 4a'^2 5a'^2 6a'^2 1a'^2.$$

The electron scattering calculations, as described above, were carried out at the static exchange level. They revealed two resonances in A' and one resonance in A'' . In A' representation in equilibrium geometry, the lower resonance energy is found to be $\epsilon_{\text{res}}^{1^2A'}(\mathbf{Q}_{\text{eq}}) = 0.1 \text{ a.u.}$ (2.71 eV) and the higher and broader resonance energy is found to be $\epsilon_{\text{res}}^{2^2A'}(\mathbf{Q}_{\text{eq}}) = 0.24 \text{ a.u.}$ (6.53 eV). These values are consistent with the π^* - and the σ^* -shape resonances observed experi-

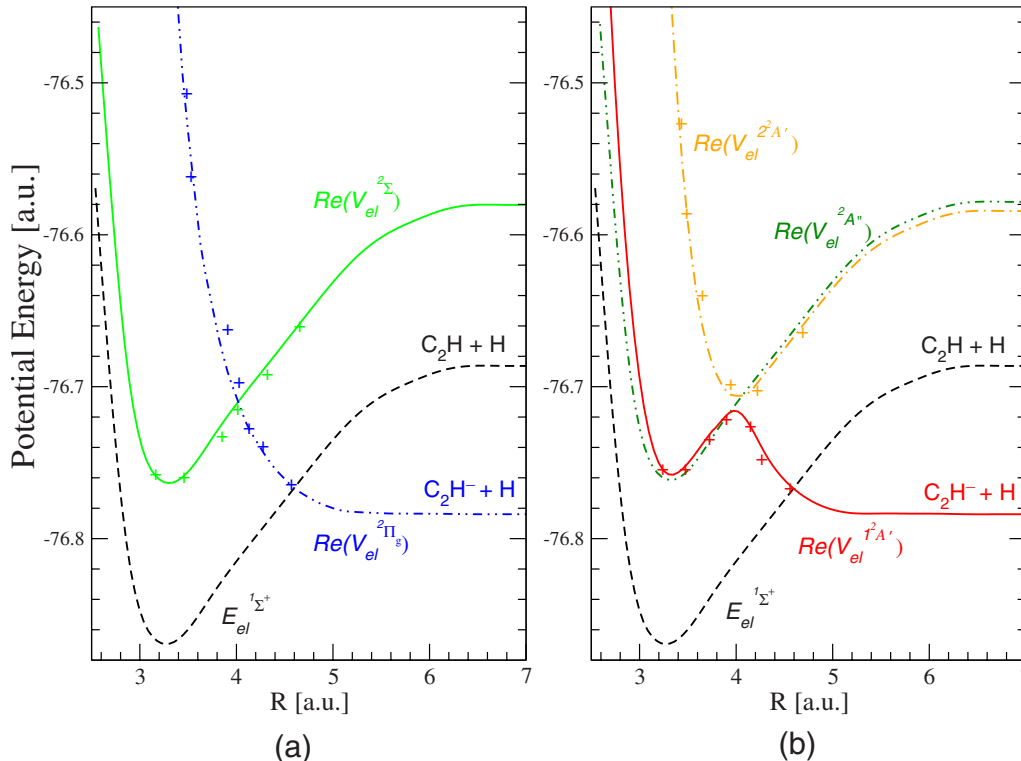


FIG. 2. (Color online) Potential energy curves in linear ($\theta=0^\circ$) (a) and quasilinear ($\theta=1^\circ$) (b) geometries. Plots in (a) show the curve crossing between $^2\Sigma$ (dotted-dotted-dashed line) and $^2\Pi_g$ (solid line) states. Plots in (b) show the lift of degeneracy of $^2\Pi_g$ state and splitting into the $1^2A'$ (solid line) and $2^2A'$ (dotted-dashed line) adiabatic manifolds. The shape of the $^2A''$ manifold (dotted-dotted-dashed line) does not vary with bending.

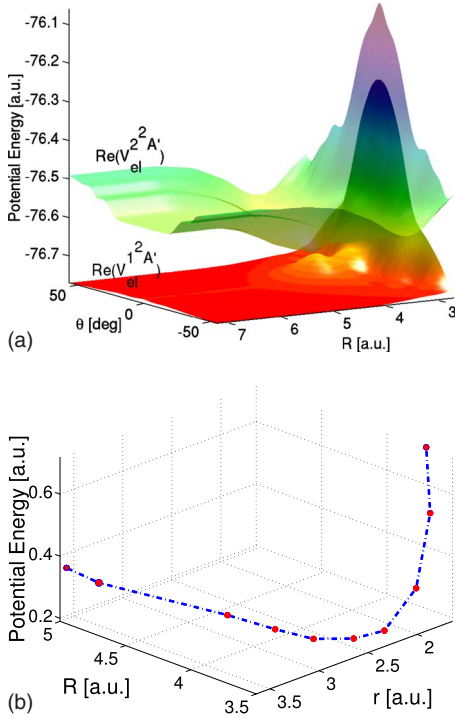


FIG. 3. (Color online) Three-dimensional plot of the real part of the resonant states $V_{el}^{1^2A'}(r=r_{eq}, R, \theta)$ (bottom surface) and $V_{el}^{2^2A'}(r=r_{eq}, R, \theta)$ (top surface) showing a conical intersection at $R=3.85$ a.u. (top panel); the seam of conical intersections as a function of (r, R) space (bottom panel).

mentally [20]. In fact, upon bending the linear molecule, the $^2\Sigma$ resonant state becomes the $2^2A'$ state and the doubly degenerate $^2\Pi_g$ resonant state splits into two manifolds denoted by $1^2A'$ and $2^2A''$ in terms of the C_s point group. Examination of the T -matrix elements for incident electron energy around 0.1 a.u. shows that those corresponding to the p -wave component dominate, hence, the electronic configuration of the π^* resonant state, which is the focus of this paper, is given by

$$(^2\Pi_g)1\sigma_g^2 1\sigma_u^2 2\sigma_g^2 2\sigma_u^2 3\sigma_g^2 1\pi_u^4 1\pi_g^1.$$

In A'' representation, we find the resonance to lie at $\epsilon_{res}^{2^2A''}(\mathbf{Q}_{eq})=0.1$ a.u. and appears to change little with change in geometry and hence will be ignored in the remainder of the present study. Figure 2 depicts the crossing between the $^2\Sigma$ and the $^2\Pi_g$ states at $R_c=3.85$ a.u. in linear geometry. Upon crossing of the neutral curve by the resonant state, the negative ion becomes bound and the system is therefore treated by electronic structure methods.

This provides the asymptotic states of $C_2H_2^*$ which we find lying at 0.10 a.u. (2.72 eV) below the (C_2H+H) neutral asymptote in linear geometry consistent with measured adiabatic electron affinity of C_2H (2.94 ± 0.1 eV) [24]. We also find a good agreement for the C–H bond dissociation energy $D_e(HC_2-H)=0.195$ a.u. (5.302 eV) compared to 529.89 ± 0.01 kJ/mol (5.49 eV) measured by Stark anti-crossing spectroscopy [25].

The second series of calculations is carried out including both R and r with $r=[C\equiv C] \in [1.6435 \text{ a.u.}, 3.6435 \text{ a.u.}]$ while maintaining the molecule in the quasilinear geometry ($\theta=1^\circ$). Thus, two-dimensional surfaces can thus be constructed in this domain as will be shown in the following section of the paper. By determining the locus of the minimum of the neutral APES, we can deduce the equilibrium geometry of the neutral molecule. The present calculations lead to $r_{eq}=[C\equiv C]_{eq}=2.29$ a.u. (1.21 Å) and $[C-H]_{eq}=2.01$ a.u. (1.06 Å) (that is $R_{eq}=3.28$ a.u.) equilibrium internuclear distances which is in good agreement with previous studies [26]. In linear geometry of C_2H_2 , the locus of the intersection points of the $^2\Sigma$ and the $^2\Pi_g$ APES forms a seam represented as a function of r and R in Fig. 3(b).

The third series of calculations involved bending the molecule by an angle θ in the interval $[1^\circ, 55^\circ]$ leading to the construction of a three-dimensional potential energy surface. One-dimensional cuts of this APES displaying the effect of bending are shown in Fig. 4.

The topology of the resonant APES in the vicinity of the resonant curve crossing exhibits a barrier with a height around 0.06 a.u. (1.63 eV) above the minimum of the $1^2A'$ states in the Frank-Condon region. This barrier decreases as the bending is increased as can be clearly seen through the three-dimensional conical intersection feature in Fig. 3(a).

The case of a nonplanar molecule was explored through an additional series of calculations where the second C–H bond is bent out of the plane of molecule by an angle β' [see Fig. 1(a)]; thus reducing the symmetry of C_2H_2 to the C_1 point group. The resulting APES for β' values of 1° , 22.5° , and 40° as a function of the distance d and for β' values of 1° and 22.5° where d' is kept constant at the equilibrium distance 2.01 a.u. are shown in Fig. 5.

No significant change of the APES structure is observed due to β and the maximum difference between the respective curves in the two calculated values of β' is found to be of the order of 4×10^{-3} a.u.

Therefore, in our present treatment, we reduced C_2H_2 to a triatomic system by considering one of the C–H groups as a single species held at the equilibrium spacing throughout. This reduces the number of internal degrees of freedom to three and makes the system dynamics amenable to a three-dimensional calculation in Jacobi coordinates on a grid inside the domain $r \in [1.6435 \text{ a.u.}, 3.6435 \text{ a.u.}]$, $R \in [2.5 \text{ a.u.}, 7.0 \text{ a.u.}]$, and $\theta \in [1^\circ, 55^\circ]$.

III. NUCLEAR DYNAMICS

A. Theory

We solve for the nuclear dynamics of the metastable negative ion state in the local complex potential model. The approximation used in this model has been discussed in detail previously [27] and will only be outlined here. The nuclear wave equation is given by

$$[E - \hat{H}(\mathbf{Q})]\xi_\nu^\Lambda(\mathbf{Q}) = \eta_\nu^\Lambda(\mathbf{Q}), \quad (4)$$

where E , the total energy of the system, is the sum of the energy of the vibrational state ν and the kinetic energy of the incident electron,

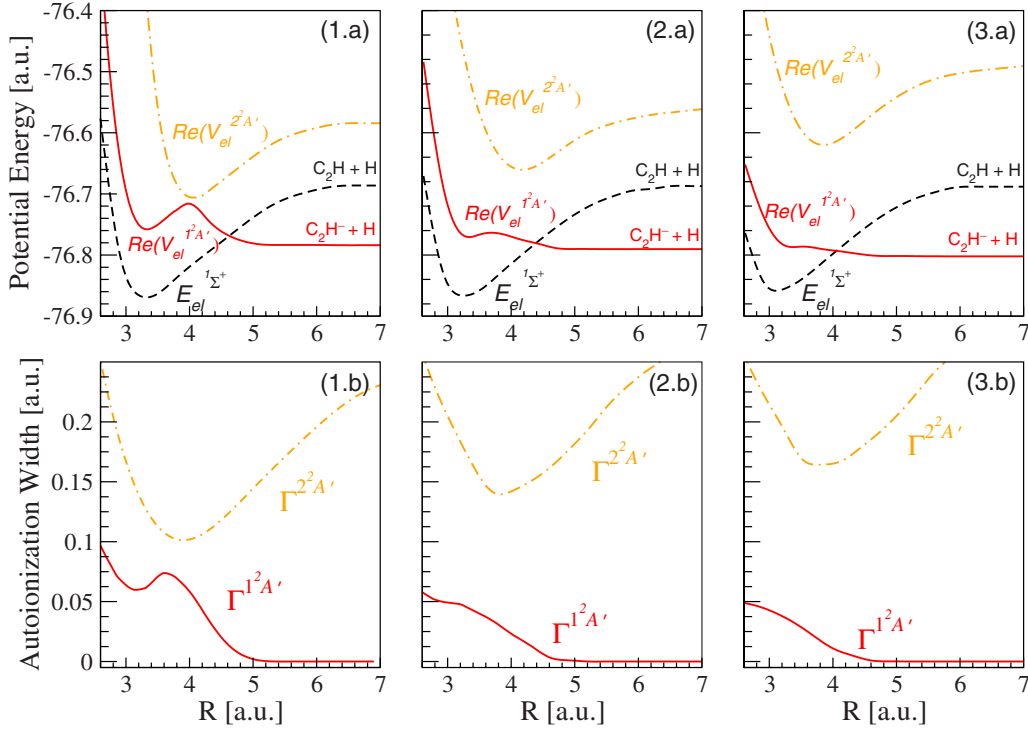


FIG. 4. (Color online) Cuts of the neutral $1^1\Sigma_g^+$ (dashed black line) and resonant $1^2A'$ (solid red line) and $2^2A'$ (dotted-dashed line) APES along the dissociative coordinate R for $r=r_{\text{eq}}$ and for bending angles $\theta=0.61^\circ$, 18.52° , and 30.49° .

$$E = E_\nu + \frac{k^2}{2}, \quad (5)$$

and the Hamiltonian operator is given by

$$\hat{H}(\mathbf{Q}) = \hat{T}_Q + V_{el}^\Lambda(\mathbf{Q}). \quad (6)$$

Here, the superscript Λ represents the irreducible representation relevant to the nuclear wave functions. The kinetic energy operator \hat{T}_Q is given in Eq. (7) for a total momentum operator $J=0$ and the potential $V_{el}^\Lambda(\mathbf{Q})$ relevant to C_2H_2^* is given by Eq. (8) (note that we use atomic units $\hbar=m_e=1$ throughout),

$$\hat{T}_Q = -\frac{1}{2\mu_r}\partial_r^2 - \frac{1}{2\mu_R}\partial_R^2 - \frac{1}{2}\left(\frac{1}{\mu_r r^2} + \frac{1}{\mu_R R^2}\right)\frac{1}{\sin\theta}\partial_\theta(\sin\theta\partial_\theta), \quad (7)$$

where μ_r and μ_R specify the reduced masses associated with the r and R coordinates,

$$V_{el}^\Lambda(\mathbf{Q}) = E_{el}^\Lambda(\mathbf{Q}) + \epsilon_{\text{res}}^\Lambda(\mathbf{Q}) - \frac{i}{2}\Gamma^\Lambda(\mathbf{Q}). \quad (8)$$

The driving term $\eta_\nu^\Lambda(\mathbf{Q})$ in Eq. (4) is defined as

$$\eta_\nu^\Lambda(\mathbf{Q}) = \left(\frac{\Gamma^\Lambda(\mathbf{Q})}{2\pi}\right)^{1/2} \chi_\nu^\Lambda(\mathbf{Q}), \quad (9)$$

where the term that multiplies $\chi_\nu^\Lambda(\mathbf{Q})$ is known as the entry amplitude and it expresses the capture probability of the incoming electron by the molecular target in the discrete vibrational state ν into the resonant state associated with the com-

plex potential of Eq. (8). Finally, $\xi_\nu^\Lambda(\mathbf{Q})$ is the nuclear wave function we seek to determine. We use the time-dependent formulation established by McCurdy and Turner [28]. The problem thus reduces to solving the time-dependent Schrödinger equation,

$$\hat{H}(\mathbf{Q})\Phi_\nu^\Lambda(\mathbf{Q}, t) = i\partial_t\Phi_\nu^\Lambda(\mathbf{Q}, t),$$

$$\Phi_\nu^\Lambda(\mathbf{Q}, 0) = \eta_\nu^\Lambda(\mathbf{Q}). \quad (10)$$

We use the a computational technique based on MCTDH formalism discussed in detail in [29]. In the context of this theory, the nuclear wave function for the negative ion of C_2H_2 is expressed in the Jacobi coordinates $\mathbf{Q}=(r, R, \theta)$ as

$$\Phi_\nu^\Lambda(r, R, \theta, t) = \sum_{i=1}^{N_r} \sum_{j=1}^{N_R} \sum_{k=1}^{N_\theta} A_{ijk}(t) \rho_i(r, t) \varrho_j(R, t) \Theta_k(\theta, t). \quad (11)$$

Each single-particle function appearing in Eq. (11) is in turn expanded in terms of a function basis set chosen to correspond to that of a discrete variable representation (DVR) for computational efficiency. Here, N_r , N_R , and N_θ are all set to the value 8 and the single-particle functions associated with the variables R , r , and θ are expressed in terms of sine-DVR (100 grid points), Hermite-DVR (50 grid points), and Legendre-DVR (94 grid points), respectively.

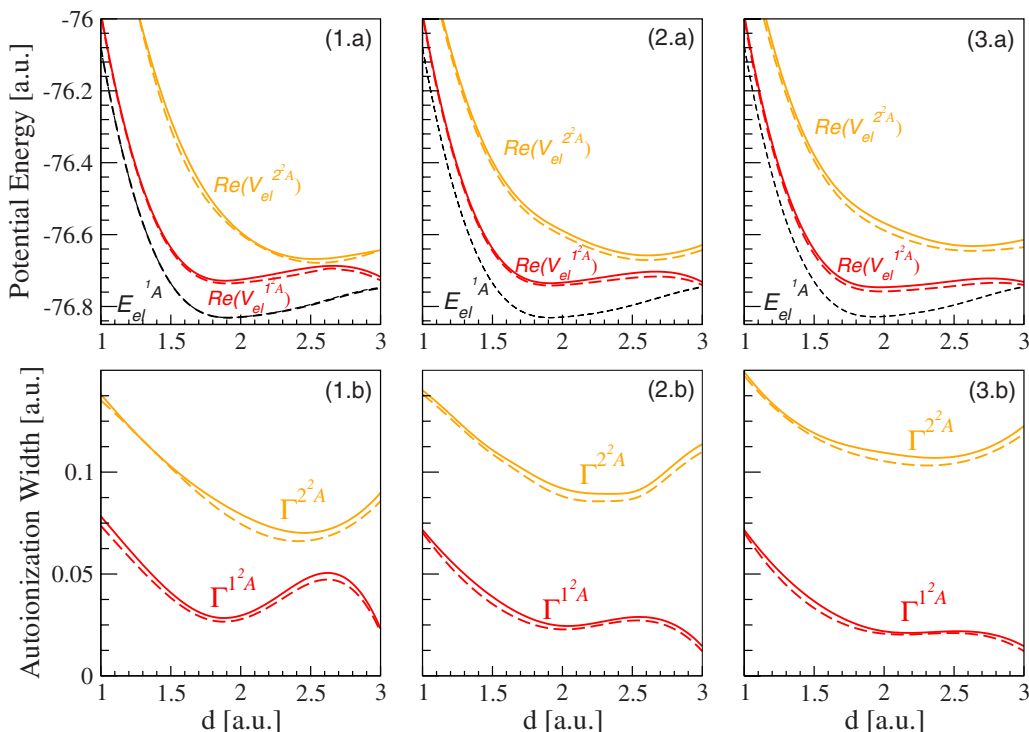


FIG. 5. (Color online) Cuts of the $1A$, 1^2A , and 2^2A APES along the dissociative coordinate R for $r=r_{\text{eq}}$ and for out-of-plane bending angles $\beta'=1^\circ$ (solid lines) and 22.5° (dashed lines) for three values of bending $\beta=1^\circ$ [plots (1a) and (1b)], $\beta=22.5^\circ$ [plots (2a) and (2b)], and $\beta=40^\circ$ [plots (3a) and (3b)].

B. Wave-packet propagation

1. Initial wave function

The construction of the APESs relevant to the neutral target and the negative ion which determine the potentials appearing in the Hamiltonian in Eq. (4) was described in the preceding sections. The nuclear wave function of the neutral target is computed using a relaxation technique implemented in the MCTDH package. This calculation yields the ground vibrational state $\chi_0^{\Sigma^+}(r, R, \theta)$ appearing in Eq. (9); the square of the magnitude of this function is represented in Fig. 6. As expected, this reduced density function is centered at the equilibrium geometry of the C_2H_2 .

2. Dissociation dynamics

By applying Eq. (9), we determine the initial wave packet needed to solve the system of Eq. (10). In this study, we consider propagation on the $1^2A'$ manifold; APES interactions and nonadiabatic effects will be investigated in future papers. Thus, in Eq. (6), the potential is given by $E_{el}^{1^2A'}(\mathbf{Q}) + \epsilon_{\text{res}}^{1^2A'}(\mathbf{Q}) - \frac{i}{2}\Gamma^{1^2A'}(\mathbf{Q})$.

Since the wave function is a function of three variables (r, R, θ) , we have chosen to show contour plots in two-dimensional slices taken with the other variable at its equilibrium value. In the left-hand column, the contour plot is shown in (R, θ) with $r=r_{\text{eq}}$. In the right-hand column, the wave function is shown as a function of r and R at $\theta=0$. Propagation is carried out for a duration of 9 fs. As can be seen in the plots of Fig. 7, there is little change in r and R

until the molecule bends. As it bends, R , that is the HCC–H distance begins to increase, leading to this bond breaking. This indicates that the molecule bends as the hydrogen atom dissociates. As can also be seen in Fig. 7, the $C\equiv C$ bond, described by the coordinate r , stretches. In this dimension, the surface is bound as depicted in the (r, R) surfaces of the right-hand column of Fig. 7. However, there is no recurrence of the wave packet in r , and hence no boomerang structure. All these observations are in agreement with findings in [11,20,21].

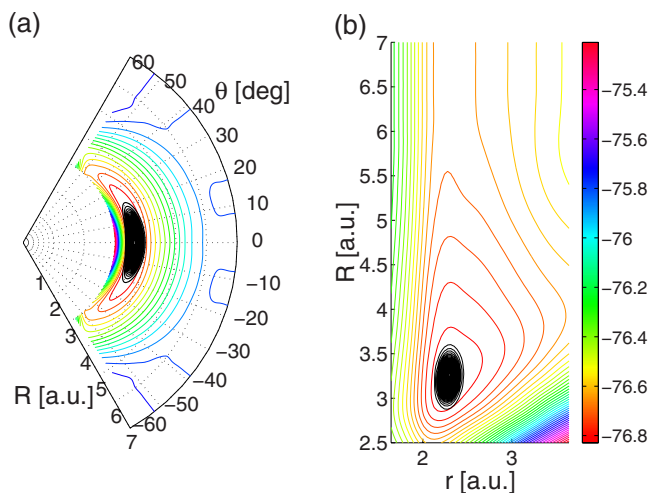


FIG. 6. (Color online) Contour plots of the ground state $E_{el}^{\Sigma^+}(\mathbf{Q})$ (color scale contours) and the ground vibrational state $\chi_{v=0}^{\Sigma^+}(\mathbf{Q})$ (black contours) in R, θ plane (a) and r, R plane (b).

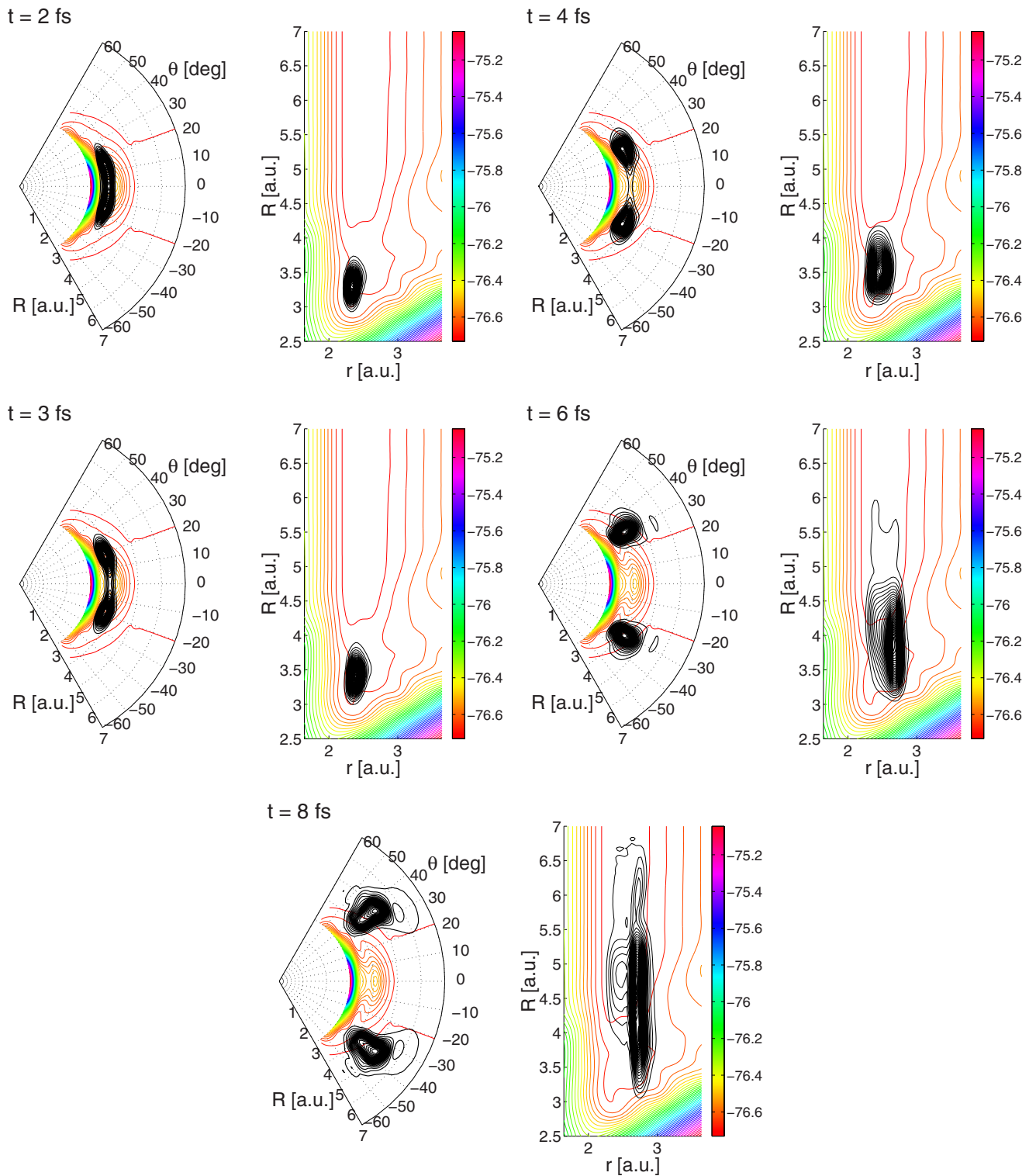


FIG. 7. (Color online) Snapshots of the wave packet (black contours) propagation on the $V_{el}^{1A'}(r, R, \theta)$ APES (color scale contours) taken at 2, 3, 4, 6, and 8 fs. The left-hand panels show the propagation on a (R, θ) polar grid (wave packet integrated over the r coordinate) and the right-hand panels show the propagation on a (r, R) grid (wave packet integrated over the θ coordinate).

C. DEA cross section

Finally, the DEA cross section is deduced from the wave-packet flux through a boundary that defines the asymptotic region for wave-packet propagation. This region is chosen

such that it decouples the rearrangement channel of interest [that is the channel given by (I)] from the other possible channels which is achieved by defining a characteristic function of the asymptotic region. The MCTDH package provides the possibility of placing a complex absorbing poten-

tial (CAP) that, if chosen appropriately, enforces the zero boundary conditions on the numerical grid. In fact, it has been demonstrated that the CAP cannot only damp the wave packet thus of reducing the effect of back-reflections but also allows efficient computation of the flux going through it (this is detailed in Refs. [32,33], and references therein). A quadratic CAP has been adopted in this study, it is given by

$$-iW^{(I)}(\mathbf{Q}) = -i\varepsilon(R - R_{\text{CAP}})^2 h^{(I)}(R - R_{\text{CAP}}), \quad (12)$$

where $h^{(I)}$ is the Heaviside step function associated with the arrangement channel (I) shifted such that the complex potential is switched on at the asymptotic value R_{CAP} taken to be 6.4 a.u. in the present calculation. The CAP strength ε must be chosen sufficiently small so the perturbation does not effect the wave packet beyond first order as discussed in [32]; here $\varepsilon = 6 \times 10^{-3}$ a.u. is considered. Note that such formulation is convenient in practice because it is independent of the choice of the shape of the boundary surface as long as it separates the arrangement channel in question. By introducing the CAP, the perturbed Hamiltonian of the system defined in Eq. (6) has the expression

$$\hat{H} = \hat{H} - iW^{(I)}(\mathbf{Q}). \quad (13)$$

We further introduce a flux operator $\hat{F}^{(I)}$ defined by

$$\hat{F}^{(I)} = i[\hat{H}, h^{(I)}], \quad (14)$$

The energy-resolved outgoing flux associated with the initial target vibrational state ν through the CAP is therefore given by

$$F_{\nu}^{(I)}(E) = \frac{1}{(2\pi)^2 |\Delta(E)|^2} \langle \xi_{\nu}^{\Lambda} | \hat{F}^{(I)} | \xi_{\nu}^{\Lambda} \rangle_{\mathbf{Q}}. \quad (15)$$

The MCTDH package implements a routine that computes $F_{\nu}^{(I)}(E)$. The term in angular brackets in Eq. (15) may be expressed in terms of the partial-wave DEA amplitude coefficients $A_l(E_{\nu} + \frac{k^2}{2})$ as

$$\langle \xi_{\nu}^{\Lambda} | \hat{F}^{(I)} | \xi_{\nu}^{\Lambda} \rangle_{\mathbf{Q}} = \frac{1}{2\pi \mu_R} \sum_l \left| A_l \left(E_{\nu} + \frac{k^2}{2} \right) \right|^2, \quad (16)$$

where κ_{ν} is the relative momentum of the dissociating fragments. In the time-dependent formulation of the dynamics, the left-hand-side term of Eq. (16) is computed in terms of the time domain integrals as

$$\langle \xi_{\nu}^{\Lambda} | \hat{F}^{(I)} | \xi_{\nu}^{\Lambda} \rangle_{\mathbf{Q}} = \int_0^{\infty} dt \int_0^{\infty} dt' \langle \eta_{\nu}^{\Lambda} | e^{i(\hat{H}^{\dagger} - E)t} \hat{F}^{(I)} e^{-i(\hat{H} - E)t'} | \eta_{\nu}^{\Lambda} \rangle_{\mathbf{Q}}. \quad (17)$$

The reader is referred to Refs. [30–33] for detailed treatment of the CAP-based flux formalism. The definition of the cross section relevant to the DEA channel (I) may be written based on partial wave formulation as

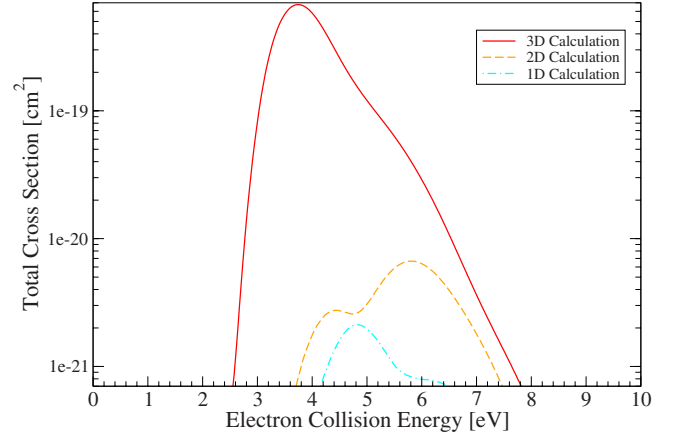


FIG. 8. (Color online) Total DEA cross section for one-dimensional [$\mathbf{Q}=(R)$], two-dimensional [$\mathbf{Q}=(r,R)$], and three-dimensional [$\mathbf{Q}=(r,R,\theta)$] calculations in logarithmic scale.

$$\sigma_{\nu \rightarrow \text{DEA}} \left(E_{\nu} + \frac{k^2}{2} \right) = g_s g_a \frac{2\pi^2}{k^2} \frac{\kappa_{\nu}}{\mu_R} \sum_l \left| A_l \left(E_{\nu} + \frac{k^2}{2} \right) \right|^2, \quad (18)$$

where the factors g_s and g_a represent, respectively, the statistical ratio of the electronic multiplicity of the resonant state to the electron multiplicity of the neutral target and the arrangement channel multiplicity; both factors are equal to two in the case of mechanism (I).

The derivation of this expression involves the expression of the molecule's nuclear coordinates in the space-fixed frame; the algebraic details of this treatment are equivalent to the case of the study of DEA to water [34]. Finally, by substituting the expression of the flux output by the flux analysis routine, a workable expression of the total DEA cross section as a function of electron collision energy is obtained,

$$\sigma_{\nu \rightarrow \text{DEA}} \left(\frac{k^2}{2} \right) = g_s g_a \frac{4\pi^3}{k^2} F_{\nu}^{(I)} \left(\frac{k^2}{2} \right). \quad (19)$$

The results are shown in Fig. 8 for three calculations, a one-dimensional calculation where only R was used, a two-dimensional calculation in r,R , that is with no bend, and finally the full three-dimensional r,R,θ results. As can be seen in Fig. 8, in the one- and two-dimensional calculations, the cross section is small and shows a threshold at much higher energy. This is due to the barrier (see Fig. 2) that exists if the molecule is not allowed to bend. When the bend is included, the cross section increases by almost two orders of magnitude and the threshold drops to 2.716 eV as is observed in experiment [20].

Figure 9 shows a comparison of the foregoing computed cross section with the experimental findings of [11,21]. Although the cross section obtained by Azria *et al.* is in fair agreement with the present results, the peak position is found to lie about 0.44 eV below the computed value and its height is slightly outside the error region. In addition, the maximum of the cross section for DEA to C_2D_2 was found to be 0.19 pm^2 by the same authors which is consistent with the pronounced isotope effect observed in the present work

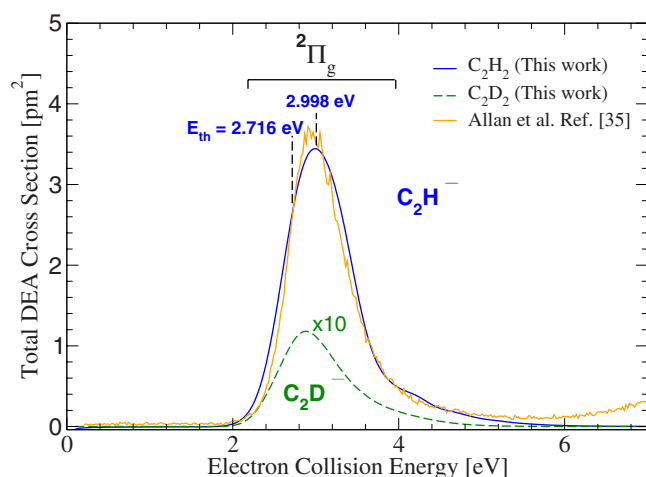


FIG. 9. (Color online) Comparison of computed total DEA cross section in the three-dimensional case to experimental results of [21]—isotope effect observed in DEA to C_2D_2 .

where the height of the cross section corresponding to C_2D^- ion yield is 0.119 pm^2 (see Fig. 9) leading to a $\sigma_{0 \rightarrow \text{DEA}}^{(C_2D^-)}(3 \text{ eV}) / \sigma_{0 \rightarrow \text{DEA}}^{(C_2H^-)}(3 \text{ eV})$ ratio of about 3.46×10^{-2} . Our theoretical cross section further shows an excellent agreement with the shape, onset, and magnitude of the recent experimental values of Allan *et al.* [21].

In order to determine the energy channeled into the negative ion fragments in the form of $C \equiv C$ vibrational modes, we project the final wave packet on the C_2H^- vibrational states. The relative population of the first eight states ($\nu' = 1, \dots, 7$) is therefore given by the branching ratios $\alpha_{\nu'}(E)$ of Eq. (20),

$$\alpha_{\nu'}\left(\frac{k^2}{2}\right) = \frac{F_{\nu\nu'}^{(1)}\left(\frac{k^2}{2}\right)}{F_{\nu}^{(1)}\left(\frac{k^2}{2}\right)}, \quad \nu' = 1, \dots, 7, \quad (20)$$

where

$$F_{\nu\nu'}^{(1)}\left(\frac{k^2}{2}\right) = \langle \xi_{\nu'}^{\Lambda'} | \hat{P}_{\nu'} \hat{F}^{(1)} \hat{P}_{\nu'} | \xi_{\nu}^{\Lambda} \rangle_{\mathbf{Q}}, \quad (21)$$

where $\hat{P}_{\nu'}$ is the projection operator on the vibrational states $\xi_{\nu'}^{\Lambda'}$ of C_2H^- , that is

$$\hat{P}_{\nu'} = |\xi_{\nu'}^{\Lambda'}\rangle\langle\xi_{\nu'}^{\Lambda'}|. \quad (22)$$

The vibrational modes $\xi_{\nu'}^{\Lambda'}$ of the ethynyl negative ion considering only the $C \equiv C$ stretch are determined by diagonalizing the associated Hamiltonian using the asymptotic poten-

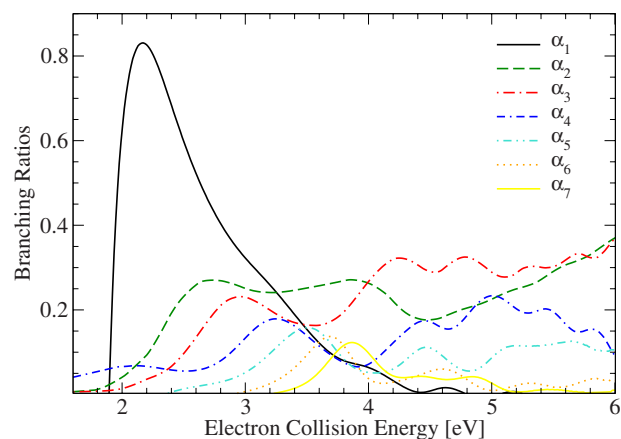


FIG. 10. (Color online) Branching ratios to the seven lowest $HC \equiv C^-$ vibrational modes.

tial at the dissociation limit ($R=6.4 \text{ a.u.}$ in the present calculation). These vibrational modes have $\Lambda' = \Sigma^+$ symmetry which leads to a nonzero overlap integral in Eq. (21). As can be seen in Fig. 10, at threshold only the ground vibrational state is populated, with all energy funneled into dissociation. At higher energies, the higher vibrational states become populated. To our knowledge, there are no experiments that address the final vibrational and rotational state of the products with which to compare.

IV. DISCUSSION AND CONCLUSION

This study demonstrates that DEA is indeed an important decay channel for the π^* resonant states formed in low-energy (below 7 eV) electron-acetylene collisions. It is clear that in this system a one-dimensional model is inadequate to describe the dissociation process. As was seen in earlier studies of formic acid [22], the molecule exhibits a complex dissociation path, involving bending as well as stretching of the $C \equiv C$ and $C-H$ bonds. Since C_2D_2 showed a significant isotope effect compared to C_2H_2 , it is likely that the singly deuterated species HCCD will also display such an effect in the dissociation. Calculations are in progress that will address this issue. There exist higher energy resonance states in this system which are believed to lead to dissociation via a vinylidene configuration to form the C_2^- ion. Future calculations will address this interesting dissociation channel.

ACKNOWLEDGMENTS

We would like to thank Michael Allan for providing his unpublished results. We acknowledge support from the National Science Foundation under Grant No. PHY-05-55401 and the U.S. DOE Office of Basic Energy Science, Division of Chemical Science.

- [1] K. S. Noll, R. F. Knacke, A. T. Tokunaga, J. H. Lacy, S. Beck, and E. Serabyn, *Icarus* **65**, 257 (1986).
- [2] J. Lequeux and E. Roofer, *Phys. Rep.* **200**, 241 (1991).
- [3] J. H. Lacy *et al.*, *Astrophys. J.* **342**, L43 (1989).
- [4] O. Abby's and D. Schulze-Makuch, *Proceedings of the Second European Workshop on Exo/Astrobiology* (Graz, Austria, 2002), pp. 16–19.
- [5] Space Explorers™, *Partial ingredients for DNA and protein found around star*, 2005, Vol. 04, issue 09.
- [6] A. H. Lettington, *Carbon* **36**, 555 (1998).
- [7] S. Stoykov, C. Eggs, and U. Kortshagen, *J. Phys. D* **34**, 2160 (2001).
- [8] M. S. Bell, K. B. K. Teo, and W. I. Wilne, *J. Phys. D* **40**, 2285 (2007).
- [9] A. N. Hayhurst and H. R. N. Jones, *Nature (London)* **296**, 61 (1982).
- [10] L. von Trepka and H. Neuert, *Z. Naturforsch. A* **18**, 1295 (1963).
- [11] R. Azria and F. Fiquet-Fayard, *J. Phys.* **33**, 663 (1972).
- [12] R. Abouaf, L. Andric, R. Azria, and M. Tronc, *Abstracts, XII ICPEAC, Gatlinburg, U.S.A., 1981* (ICPEAC, Gatlinburg, 1981), p. 409.
- [13] L. Andric and R. I. Hall, *Abstracts, XI Symposium on the Physics of Ionized Gases (SPIG)* (Dubrovnik, Yugoslavia, 1982), p. 83; L. Andric and R. I. Hall, *Invited Lecture, XII SPIG* (Sibevnik, Yugoslavia, 1984).
- [14] M. Tronc and L. Malegat, "Photophysics and photochemistry above 6 eV," in *Proceedings of Bordeaux Conference*, edited by F. Lahmani (Elsevier, Amsterdam, 1985), p. 203.
- [15] K.-H. Kochem, W. Sohn, K. Jung, H. Ehrhardt, and E. S. Chang, *J. Phys. B* **18**, 1253 (1985).
- [16] J. A. Tossell, *J. Phys. B* **18**, 387 (1985).
- [17] V. Krumbach *et al.*, *J. Phys. B* **22**, 4001 (1989).
- [18] F. A. Gianturco and T. Stoecklin, *J. Phys. B* **27**, 5903 (1994).
- [19] A. Jain, *J. Phys. B* **26**, 4833 (1993).
- [20] R. Dressler and M. Allan, *J. Chem. Phys.* **87**, 4510 (1987).
- [21] O. May, J. Fedor, B. C. Ibanescu, and M. Allan (unpublished).
- [22] T. N. Rescigno, C. S. Trevisan, and A. E. Orel, *Phys. Rev. Lett.* **96**, 213201 (2006).
- [23] T. N. Rescigno, B. H. Lengsfeld, and C. W. McCurdy, in *Modern Electronic Structure Theory*, edited by D. R. Yarkony (World Scientific, Singapore, 1995), Vol. 1, p. 501.
- [24] B. K. Janousek, J. I. Brauman, and J. Simons, *J. Chem. Phys.* **71**, 2057 (1979).
- [25] P. G. Green, James L. Kinsey, and R. W. Field, *J. Chem. Phys.* **91**, 5160 (1989).
- [26] S. Zou and J. M. Bowman, *Chem. Phys. Lett.* **368**, 421 (2003).
- [27] T. F. O'Malley, *Phys. Rev.* **150**, 14 (1966).
- [28] C. W. McCurdy and J. L. Turner, *J. Chem. Phys.* **78**, 6773 (1983).
- [29] G. A. Worth, M. H. Beck, A. Jäckle, and H.-D. Meyer, The MCTDH Package, version 8.2, 2000; H.-D. Meyer, The MCTDH Package, version 8.3, 2000; <http://www.pci.uni-heidelberg.de/tc/usr/mctdh/>
- [30] M. H. Beck, A. Jäckle, G. A. Worth, and H.-D. Meyer, *Phys. Rep.* **324**, 1 (2000).
- [31] H.-D. Meyer and G. A. Worth, *Theor. Chem. Acc.* **109**, 251 (2003).
- [32] U. V. Riss and H.-D. Meyer, *J. Phys. B* **26**, 4503 (1993).
- [33] A. Jäckle and H.-D. Meyer, *J. Chem. Phys.* **105**, 6778 (1996).
- [34] D. J. Haxton, Z. Zhang, H.-D. Meyer, T. N. Rescigno, and C. W. McCurdy, *Phys. Rev. A* **69**, 062714 (2004).